International Journal for Computational Civil and Structural Engineering, 17(3) 102–113 (2021)

DOI:10.22337/2587-9618-2021-17-3-102-113

# STATIC BENDING STRENGTH OF SANDWICH COMPOSITE PLATES WITH TETRACHIRAL HONEYCOMBS

***Alexey V. Mazaev, Marina V. Shitikova***

Voronezh State Technical University, Voronezh, RUSSIA
Research Institute of Building Physics of Russian Academy of Architecture and Construction Sciences, Moscow, RUSSIA

**Abstract**: The article presents a numerical strength analysis of sandwich plates with solid face layers and tetrachiral honeycomb core layer under static bending conditions. An aluminum alloy was chosen as the material of plates. For honeycomb core layers, the discretization (number of unit cells) and the relative density were varied with a constant thickness. Calculations were performed for the case of bending with rigidly clamped ends and three-point bending within the framework of the theory of elasticity by the finite element method. The strength analysis enables one to determine the load values, at which the maximal stresses according to the von Mises criterion were equal to the conventional yield stress of the material. The aim of this work is to study the effect of discretization and relative density of honeycomb core layers of tetrachiral type on the strength of sandwich plates.

**Keywords**: composite plates, tetrachiral honeycombs, multilayer plates, strength analysis, static bending, finite element method

# ПРОЧНОСТЬ СЛОИСТЫХ КОМПОЗИТНЫХ ПЛАСТИН С ТЕТРАКИРАЛЬНЫМИ СОТАМИ ПРИ СТАТИЧЕСКОМ ИЗГИБЕ

***А.В. Мазаев, М.В. Шитикова***

Воронежский государственный технический университет, г. Воронеж, РОССИЯ
Научно-исследовательский институт строительной физики РААСН, г. Москва, РОССИЯ

**Аннотация**: В работе производился численный анализ прочности слоистых композитных пластин со сплошными внешними слоями и сотовой прослойкой тетракирального типа в условиях статического изгиба. В качестве материала пластин выбран алюминиевый сплав. У сотовых прослоек варьировалась дискретизация (количество элементарных ячеек) и относительная плотность при постоянной толщине. Расчеты производились при жестком защемлении с торцов и трехточечном изгибе в рамках теории упругости методом конечных элементов. В процессе анализа прочности определялись значения нагрузки, при которых максимальные напряжения по критерию Мизеса приравнивались к условному пределу текучести материала. Целью работы является изучение влияния дискретизации и относительной плотности сотовых прослоек тетракирального типа на прочность композитных пластин.

**Ключевые слова:** композитные пластины, тетракиральные соты, многослойные пластины, анализ прочности, статический изгиб, метод конечных элементов

## 1. INTRODUCTION

In the last three decades, much attention has been paid to materials with negative Poisson's ratio, which are called auxetics [1-3]. These materials have a non-standard deformation mechanism, namely: they expand with tension and contract with compression. Despite the recent special attitude to auxetic materials, the theoretical admissibility of the existence of such materials was first shown by Love more than 120 years ago [4]. Later, Landau came to the similar conclusion [5]. Based on the well-known expression for the shear modulus for an isotropic material, it follows that when Poisson's ratio tends to -1, the shear resistance increases significantly, which is an important property for many applications. Currently, it is known about many advantages of auxetics over materials with classical behavior [6], for example: increased resistance to indentation, resistance to the process of initiation and opening of cracks, increased energy absorption, etc. Such properties of auxetics remarkably complement the properties of classical materials in composite structures, in particular, layered plates.

Honeycomb structures of certain geometry are most often used as auxetic in sandwich composites. Prall and Lakes [7] theoretically and experimentally determined negative Poisson's ratio in trichiral honeycomb structures. They also showed that Young moduli of chiral honeycombs depend on the ratio of the length of tangentially attached ribs and the radius of the cylinders, as well as on the ratio of the distance between the centers of adjacent cylinders (connected by ribs) and the radius of the cylinders. Scarpa and Tomlinson [8] theoretically assumed that re-entrant honeycomb core layers with negative Poisson's ratio increase the flexural stiffness of composite plates. They also suggested using honeycomb core layers to design composites with pre-tuned mechanical properties by changing the geometric parameters of the unit cells.

Alderson et al. [9] numerically and experimentally determined Poisson's ratios for chiral honeycombs of various types (hexa-, tetra-, antitetra-, tri- and antitri- chiral cells) under plane uniaxial compression. Honeycombs differ in the number of tangentially attached ribs, and in antichiral structures, adjacent unit cells have mirror symmetry. Alderson et al. [9] used finite element modeling and ambient experiments, in so doing prototypes were made from nylon using additive technologies. It is shown that the chiral honeycombs family has a negative Poisson's ratio. However, the trichiral structure showed a positive Poisson's ratio, and the antitrichiral structure showed auxetic behavior with short tangentially attached ribs and classic behavior with long ribs. It was showed that chiral structures, in comparison with antichiral structures, have a higher Young modulus under plane uniaxial compression for any number of ribs.

Lira et al. [10] have shown numerically and experimentally that an auxetic honeycomb structure of the re-entrant type has an increased specific flexural stiffness relative to hexagonal honeycombs. Such a structure with a reduced mass also allows one to obtain the same first natural frequency in comparison with hexagonal cells. Li and Wang [11] made sandwich composites with various honeycomb core layers: truss type, conventional honeycombs, and re-entrant honeycombs. It has been shown [11] that under the three-point bending, sandwich composites with a re-entrant type auxetic honeycombs exhibit high energy absorption and more efficient stress distribution before failure.

Alomarah et al. [12] numerically and experimentally investigated popular auxetic honeycomb structures under plane uniaxial compression: re-entrant, tetrachiral and antitetrachiral. They also investigated a new honeycomb structure, namely: re-entrant chiral. The prototypes were made of polyamide using additive technologies. Alomarah et al. [12] obtained the stress-strain curves, showed the strain modes of the investigated structures,

investigated energy absorption, and determined the magnitudes of the negative Poisson's ratio.

Xiao et al. [13] numerically and experimentally investigated the behavior of a rigidly fixed sandwich beam with re-entrant honeycombs under conditions of a local shock pulse. The deformation of the facial sheets and the auxetic core layer was also analyzed. The composites were made of an aluminum alloy using additive manufacturing. It has been experimentally shown [13] that re-entrant honeycombs with thin walls exhibit local densification in composites due to the negative Poisson's ratio. Re-entrant honeycombs with thick walls showed only global deformation without auxetic behavior.

Essassi et al. [14] experimentally and numerically investigated sandwich composites with re-entrant honeycomb core layers under three-point bending conditions. The composites were made of biological material using additive technologies. During manufacturing, the relative density of the honeycomb structure was varied. Flexural stiffness, shear stiffness and shear modulus for the sandwich composites under investigation were determined, and the effect of the relative density of the core layers on these values was evaluated.

Composite panels with auxetic honeycombs under three-point bending have been investigated in [15, 16]. The composites were made of wood-based materials. The authors determined the stiffness, strength and energy absorption capacity of the composite panels. It has been shown that sandwich panels with auxetic honeycombs have advantages over those with classical honeycombs, in so doing the plane of honeycomb core layers with auxetic behavior is oriented parallel and perpendicular to the plane of composite panels, respectively, in [10, 15-16] and [11, 13].

In the present paper, three-layer sandwich plates with solid face layers and tetrachiral honeycomb core layer under static bending are investigated numerically.

## 2. FORMULATION OF THE PROBLEM

Let us consider a honeycomb structure consisting of ordered cylinders arranged in a square grid pattern, which are connected to each other by tangentially attached ribs, where each of the cylinders contains four attached ribs (Fig. 1). It has been shown experimentally [9, 12] that tetrachiral honeycombs exhibit auxetic behavior in the plane. In the sandwich plates under consideration, the plane of honeycomb core layers with auxetic behavior is oriented parallel to the plane of the plates.

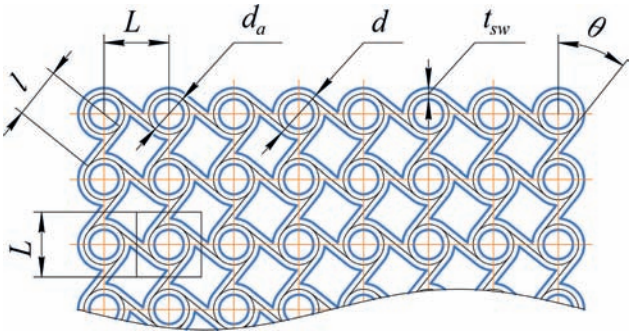


*Figure 1. Parameters of the honeycomb structure of tetrachiral type*

For numerical experiments, tetrachiral honeycombs have been designed with different discretization (number of unit cells) and equal relative density $\rho_r$, which is defined as the ratio of the volume of solid body of the honeycombs to the volume of the central layer of composites along the outer faces. The honeycombs have been considered with four values of the size of elementary cells $L = 1.6 d_a$, where $d_a \in$ 1, 1.3, 1.6, and 1.9. The volume of a solid body of the honeycomb structures could be varied by changing the thickness of their walls $t_{sw}$. For each discretization of the structure, 9 honeycomb models have been constructed with the equal step of increasing volume. At each of the four values of *L*, the tetrachiral honeycombs uniformly fill the central layer of the composites. For the obtained honeycombs, the following geometric parameters have been used:

$r_a/l = \text{const}$ $(r_a = d_a/2)$, $\theta = \text{const}$; at $\rho_r = \text{const}$, $\alpha = l/r \approx \text{const}$ $(r = d/2)$, and $\beta = t_{sw}/r \approx \text{const}$. The total thickness of the sandwich plates is 2 mm, the thickness of the face layers is 0.5 mm, and the thickness of the honeycomb core layers is 1 mm. For comparative analysis, 11 models of solid plates have been considered with an equal step of increasing volume by changing the thickness of plates from 1 to 2 mm with a step of 0.1 mm. Strength calculations for composite and solid plates have been carried out within the framework of elasticity theory by the finite element method using the «Structural Mechanics» module [17] from the «COMSOL Multiphysics 5.6» numerical simulation system.

A linear elastic body model is used to describe the behavior of the plate's material. Under the conditions of bending of composite and solid plates with rigid fixation, the displacements of nodes (Fig. 2) have been subjected to the following boundary conditions:

$$\begin{aligned} &u_{x,y,z}\left(0 \le x \le x_1, y = 0, 0 \le z \le h\right) = 0, \\ &u_{x,y,z}\left(x_2 \le x \le a, y = 0, 0 \le z \le h\right) = 0, \\ &u_{x,y,z}\left(0 \le x \le x_1, y = b, 0 \le z \le h\right) = 0, \\ &u_{x,y,z}\left(x_2 \le x \le a, y = b, 0 \le z \le h\right) = 0. \end{aligned} \quad (1)$$

Under the conditions of three-point bending of the plates, the displacements of nodes on straight line segments have been supposed as

$$\begin{aligned} &u_{x,y,z}\left(x = x_1, y = 0, 0 \le z \le h\right) = 0, \\ &u_{x,y,z}\left(x = x_2, y = 0, 0 \le z \le h\right) = 0. \end{aligned} \quad (2)$$

The plate is subjected to the external load $F_y$ uniformly distributed over a straight line segment (Fig. 2):

$$F_y = F_y\left(x = l_1, y = b, 0 \le z \le h\right), \quad (3)$$

where $a = 54$ mm and $h = 13$ mm are plate dimensions, $b = 2$ mm is its thickness, $l_1 = a/2$ mm, $x_1 = 12$ mm, and $x_2 = 42$ mm. To exclude the deflection in the *zy*-plane, the displacements of nodes in the face layers of composites and solid plates have been considered as $u_z = 0$.

The finite element mesh of the composite plates is constructed separately for each layer:

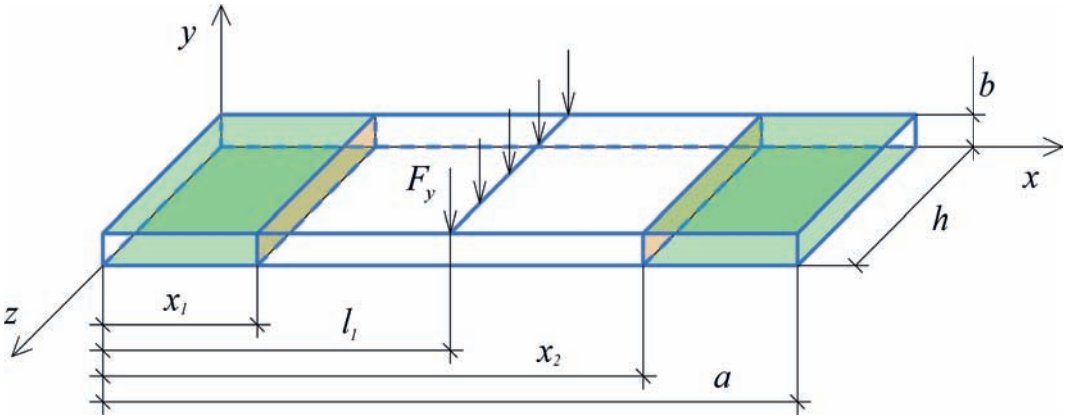


*Figure 2. Boundary conditions of composite and solid plates*

quadrangular prisms and triangular prisms are used for solid layers and honeycomb core layers, respectively (Fig. 3). The condition of continuity of field variables is established at the layer interfaces of composite plates. Figure 4 shows a finite element mesh of unit cells of tetrachiral structures at each step of increasing relative density. For constructing the mesh for solid plates, quadrilateral prisms have been

used. Finite elements of the serendipity family of the second order are used in all models.

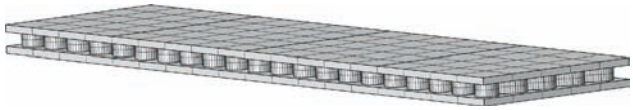

*Figure 3. Mesh of finite elements of composite plates*

The properties of the D16 aluminum alloy [18] are used as the material properties of composite and solid plates, namely: Poisson's ratio $\mu = 0.33$, elastic modulus $E = 72$ GPa, density $\rho = 2780$ kg/m$^3$, and the conventional yield point $\sigma_{0.2} = 290$ MPa.

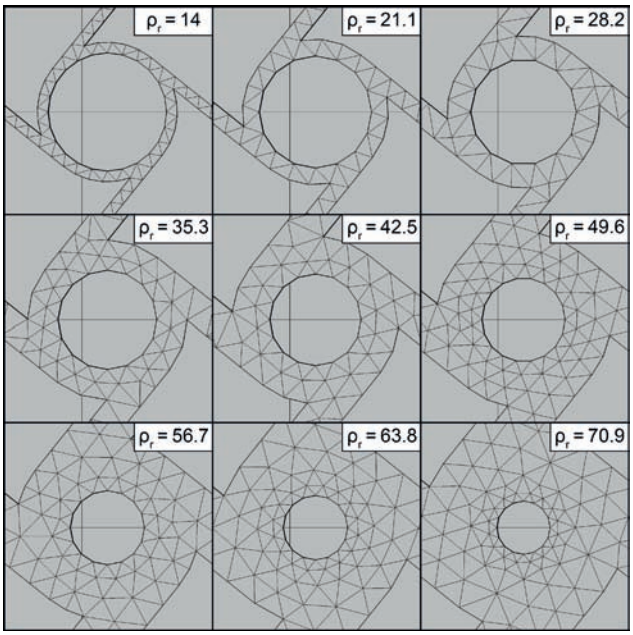


*Figure 4. Finite element mesh of unit cells of tetrachiral structures*

During static bending of composite and solid plates, the load values $F_y$ (N) have been determined, at which the maximum stresses according to the von Mises criterion are equal to the conventional yield stress of the material $\sigma_{max} = \sigma_{0.2}$.

In order to verify the results of calculations via the «COMSOL» system, additional calculations of solid plates have been performed by the finite element method in displacements using the algorithm for solving the plane problem based on the known equations of theory of elasticity [19-20], adopting the following boundary conditions (Fig. 2):

$$\begin{aligned} u_{x,y,z}\left(x = x_1, 0 \le y \le b, 0 \le z \le h\right) = 0, \\ u_{x,y,z}\left(x = x_2, 0 \le y \le b, 0 \le z \le h\right) = 0. \end{aligned} \tag{4}$$

In the case of the three-point bending of the plates, the boundary conditions (2) and (3) have been used.

The algorithm for solving the plane problem was adapted for plate calculations, in so doing the stiffness matrix of the finite element $k^e$ is determined by the expression

$$k^e_{r,s} = k^E_{r,s} + k^G_{r,s}, \tag{5}$$

where the submatrix of normal deformations $k^E$ and the submatrix of shear deformations $k^G$ have the following form:

$$k^E_{r,s} = \frac{Eh}{4(1+\mu)(1-2\mu)} \cdot (1-\mu) \cdot \begin{bmatrix} \gamma\xi_r\xi_s\left(1+\frac{\eta_r\eta_s}{3}\right) & \frac{\mu\xi_r\eta_s}{(1-\mu)} \\ \frac{\mu\eta_r\xi_s}{(1-\mu)} & \frac{\eta_r\eta_s}{\gamma}\left(1+\frac{\xi_r\xi_s}{3}\right) \end{bmatrix}, \tag{6}$$

$$k^G_{r,s} = \frac{Gh}{4} \cdot \begin{bmatrix} \frac{\eta_r\eta_s}{\gamma}\left(1+\frac{\xi_r\xi_s}{3}\right) & \eta_r\xi_s \\ \xi_r\eta_s & \gamma\xi_r\xi_s\left(1+\frac{\eta_r\eta_s}{3}\right) \end{bmatrix}, \tag{7}$$

$G = E/2(1+\mu)$ is the shear modulus, $r$ and $s$ are numbers of matrix blocks ($r = 1, 2 \ldots 4$,

$s = 1,2\ldots 4$), $a_{fe}$ and $b_{fe}$ are dimensions of the sides of the rectangular finite element along the *x*- and *y*-axes, respectively, *h* is the size of the finite element along *z* axis, $\gamma = b_{fe}/a_{fe}$ is the dimensionless parameter, $\xi_r$, $\xi_s$ and $\eta_r$, $\eta_s$ are dimensionless coordinates of the rectangular element, which take on the following magnitudes: $\xi_1 = -1$, $\eta_1 = -1$, $\xi_2 = 1$, $\eta_2 = -1$, $\xi_3 = 1$, $\eta_3 = 1$, $\xi_4 = -1$, $\eta_4 = 1$.

The matrix *N* matching the global numbers of nodes to the local numbers is constructed according to the rule $N_{m,i} = q$ with $m \in 1,2\ldots m_f$, $i \in 1,2\ldots i_f$, and $q \in 1,2\ldots 4$, where *m* is the global node number (Fig. 5, a), $m_f$ is the quantity of global nodes, *i* is the finite element number (Fig. 5, b), $i_f$ is the quantity of finite elements, and *q* is the local number of the node of the *i*-th finite element (Fig. 6), in so doing if $N_{m,i} \notin q$, then $N_{m,i} = 0$.

$r = N_{m,i}$, $s = N_{n,i}$, $m,n \in 1,2\ldots m_f$, if $r \vee s = 0$ then $k^e_{r,s} = \begin{pmatrix} 0 & 0 \\ 0 & 0 \end{pmatrix}$.

The stiffness matrix of the finite element model *K* is determined by summing the extended stiffness matrices $K = \sum_i k^{exp}(i)$. To consider the external fixation of the finite element model node, it is necessary to delete the rows $i_1 = 2m_p - 1$, $i_2 = 2m_p$ and columns $j_1 = 2m_p - 1$, $j_2 = 2m_p$ of the stiffness matrix *K*, where $m_p$ is the number of the fixed node.

The displacements of nodes are determined by the expression

$$u_a = K_a^{-1} \cdot P_a, \tag{8}$$

where $K_a^{-1}$ is the inverse stiffness matrix with due account for the fixed nodes, $P_a = \left\{ P^x_{a_1} \quad P^y_{a_2} \quad \cdots \quad P^x_{a_{c-1}} \quad P^y_{a_c} \right\}$ is the vector of nodal forces (hereinafter, the row matrix in

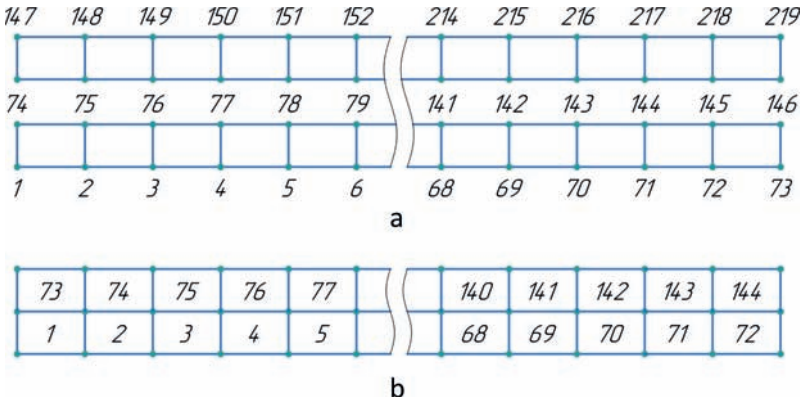


*Figure 5. Scheme of finite elements of the plate: (a) global numbering of nodes, (b) numbering of finite elements*

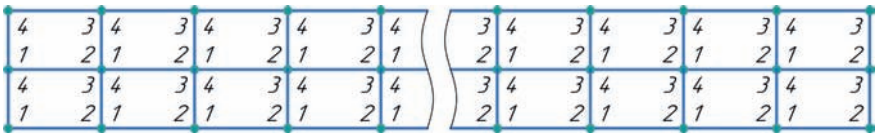

*Figure 6. Scheme of local numbering of nodes of finite elements*

The extended stiffness matrix $k^{exp}$ is constructed according to the $k^{exp}_{m,n}(i) = k^e_{r,s}$ principle, where curly braces means the column matrix), $c = 2\left(m_f - p\right)$, $P^x_{a_{c-1}}$ and $P^y_{a_c}$ are nodal forces

along *x*- and *y*-axes, respectively, and *p* is the quantity of the fixed nodes.

The full vector of displacements $u=\left\{u_1^x \quad u_2^y \quad \cdots \quad u_{e-1}^x \quad u_e^y\right\}$ $(e=2m_f)$ includes zero displacements $u_{k_o}=0$, $o\in 1,2$, where $k_1=2m_p-1$, $k_2=2m_p$, and the matrix $u_a=\left\{u_{a_1}^x \quad u_{a_2}^y \quad \cdots \quad u_{a_{c-1}}^x \quad u_{a_c}^y\right\}$ is a submatrix of *u*, where $u_{a_c}\neq 0$.

The vectors of displacements along *x*- and *y*-axes are determined by the expressions $u_m^x=u_{m_x}$ and $u_m^y=u_{m_y}$ respectively, where $m_x=2m-1$, $m_y=2m$.

The displacement vector *v* of the nodes of the *i*-th finite element is constructed as $v_i=\left\{u_{m^1}^x \quad u_{m^1}^y \quad u_{m^2}^x \quad u_{m^2}^y \quad u_{m^3}^x \quad u_{m^3}^y \quad u_{m^4}^x \quad u_{m^4}^y\right\}$, where $N_{m^1,i}=1$, $N_{m^2,i}=2$, $N_{m^3,i}=3$, $N_{m^4,i}=4$, $u_{m^q}^x$ and $u_{m^q}^y$ are the nodal displacements along *x*- and *y*-axes, respectively.

The strain vector $\varepsilon$ of the *i*-th finite element is determined from the expression

$$\varepsilon\left(i,\xi,\eta\right)=\beta\left(\xi,\eta\right)\cdot v_i, \tag{9}$$

where $\beta(\xi,\eta)$ is the matrix of the relationship between nodal displacements and deformations,

$$\beta(\xi,\eta)=\frac{1}{2}\begin{pmatrix} b_a\left(1,\eta\right) & 0 \\ 0 & a_a\left(1,\xi\right) \\ b_a\left(2,\eta\right) & 0 \\ 0 & a_a\left(2,\xi\right) \\ b_a\left(3,\eta\right) & 0 \\ 0 & a_a\left(3,\xi\right) \\ b_a\left(4,\eta\right) & 0 \\ 0 & a_a\left(4,\xi\right) \end{pmatrix}^T, \tag{10}$$

with $a_a(q,\xi)=\eta_q\left(1+\xi_q\xi\right)\big/b_{fe}$,

$b_a(q,\eta)=\xi_q\left(1+\eta_q\eta\right)\big/a_{fe}$, and $q=1,2\ldots 4$.

The vector of nodal stresses $\sigma$ of the *i*-th finite element is determined as

$$\sigma\left(i,\xi,\eta\right)=\chi\varepsilon\left(i,\xi,\eta\right), \tag{11}$$

where $\chi$ is the matrix of elastic constants, $\xi=\xi_q$, $\eta=\eta_q$, and

$$\chi=\frac{E}{\left(1+\mu\right)\left(1-2\mu\right)}\begin{pmatrix} 1-\mu & \mu \\ \mu & 1-\mu \end{pmatrix}, \tag{12}$$

The equivalent stresses $\sigma_e$ at nodes of the finite element are determined by the von Mises criterion [21]

$$\sigma_e=\sqrt{\sigma_1^{\,2}+\sigma_2^{\,2}-\sigma_1\cdot\sigma_2}, \tag{13}$$

where $\sigma_1$ and $\sigma_2$ are the principal stresses.

## 3. RESULTS

Diagrams of the stress distribution in solid plates obtained in the «Structural Mechanics» module of the «COMSOL» package have been verified using the algorithm for solving the plane problem. Based on the calculated results for the solid plate with the thickness $t=1.5$ mm using the constructed algorithm and boundary conditions (4), a graph of isolines with the stress distribution is shown in Fig. 7, a. A similar stress distribution diagram obtained in the COMSOL software with the boundary conditions (1) is presented in Fig. 7, b. The load magnitudes according to the constructed algorithm at $\sigma_{max}=\sigma_{0.2}$ for plates with the thickness $t=1.5$ and $t=2$ mm are 435 and 785.5 N, respectively, and those obtained via the COMSOL software for the same plates are 425.7 and 755.9 N, respectively. The solutions according to the two approaches are in good agreement.

The stress distribution diagrams under the condition of the three-point bending (2) for a plate with the thickness $t=1.5$ mm obtained via the algorithm for solving the plane problem and

the «COMSOL» system are presented, respectively, in Fig. 8, a and Fig. 8, b. The load magnitudes calculated via the constructed algorithm for plates with the thickness $t = 1.5$ and $t = 2$ mm at $\sigma_{max} = \sigma_{0.2}$ are 282.4 and 505.8 N, respectively, and for the same plates via the COMSOL package are 307.7 and 558.2 N, respectively. The solutions obtained using the two approaches are in good agreement.

Based on the results of the strength analysis, graphs of the sandwich plate honeycomb core relative density dependence of the load $F_y$ are shown in Fig. 9 and Fig. 10, respectively, for the boundary conditions (1) and (2). The solid body volume of composite and solid plates dependence of the load $F_y$ at bending with rigid fixation (Fig. 11) and three-point bending (Fig. 12) are also presented.

Reference to Fig. 9 shows that under the conditions of bending with rigid fixation (1), within the range of values of the honeycomb core relative density from 20 to 35 %, there is a significant difference in the strength of sandwich plates with different discretization of tetrachiral structures at the same relative density. From Fig. 10 it is seen that under the conditions of three-point bending (2), sandwich plates with different discretization and equal relative density of tetrachiral honeycombs demonstrate a small difference in the strength over the entire range of values of the relative density. Composite plates with tetrachiral honeycombs (Figs. 11-12) could significantly reduce the volume of a solid body relative to solid plates with equal strength.

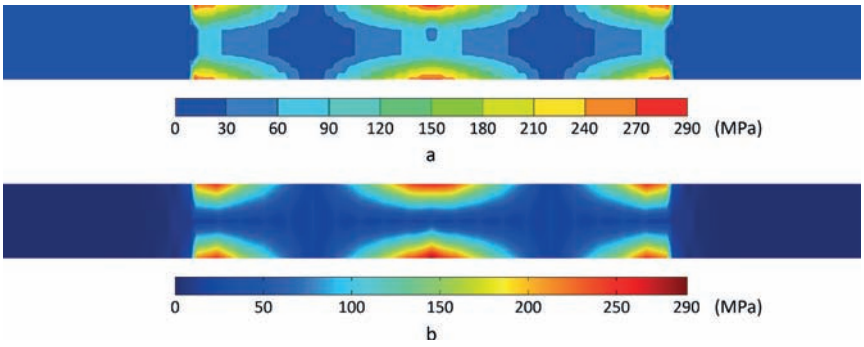


*Figure 7. The stress distribution diagrams for a solid plate with thickness $t = 1.5$ mm under the bending with rigid fixation conditions at $\sigma_{max} = \sigma_{0.2}$ obtained using (a) the algorithm for solving the plane problem, and (b) the «COMSOL» software*

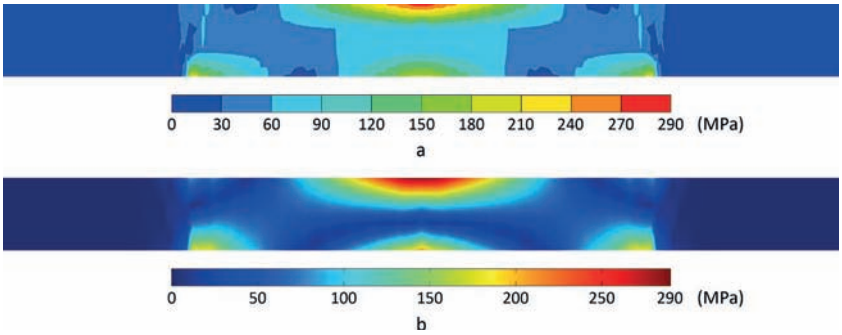


*Figure 8. The stress distribution diagrams for a solid plate with thickness $t = 1.5$ mm under the three-point bending conditions (2) at $\sigma_{max} = \sigma_{0.2}$ obtained using (a) the algorithm for solving the plane problem, and (b) the «COMSOL» software*

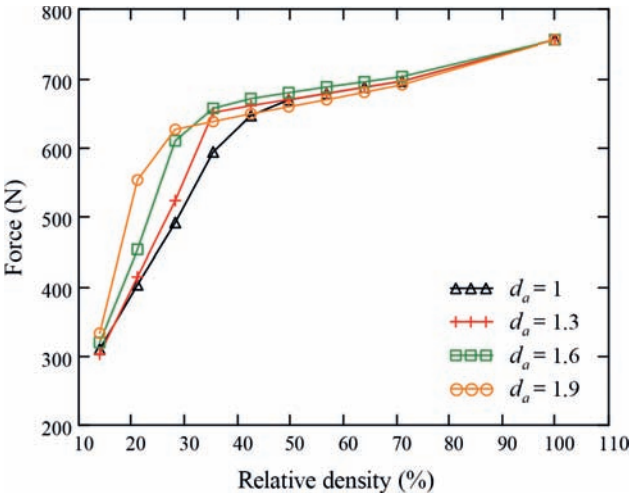


*Figure 9. Diagram of the sandwich plate honeycomb core relative density dependence of the load $F_y$ (at $\sigma_{max} = \sigma_{0.2}$) at bending with rigid fixation* (1)

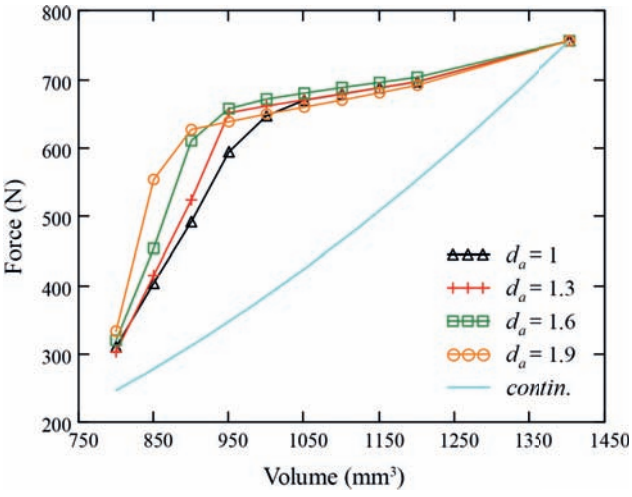


*Figure 11. Diagram of the solid body volume of composite and solid plates dependence of the load $F_y$ (at $\sigma_{max} = \sigma_{0.2}$) under bending with rigid fixation* (1)

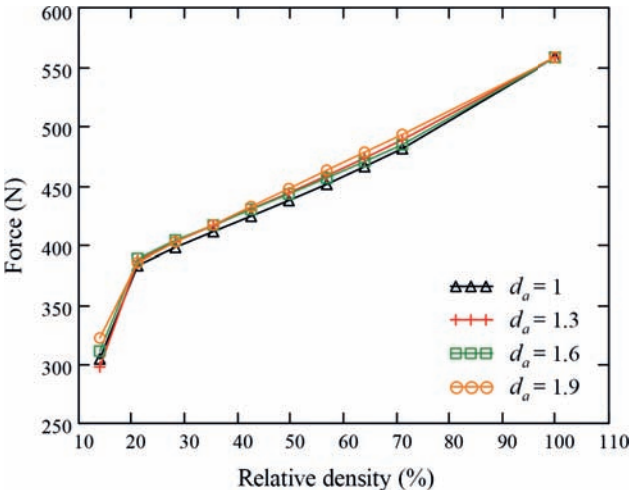


*Figure 10. Diagram of the sandwich plate honeycomb core relative density dependence of the load $F_y$ (at $\sigma_{max} = \sigma_{0.2}$) at three-point bending* (2)

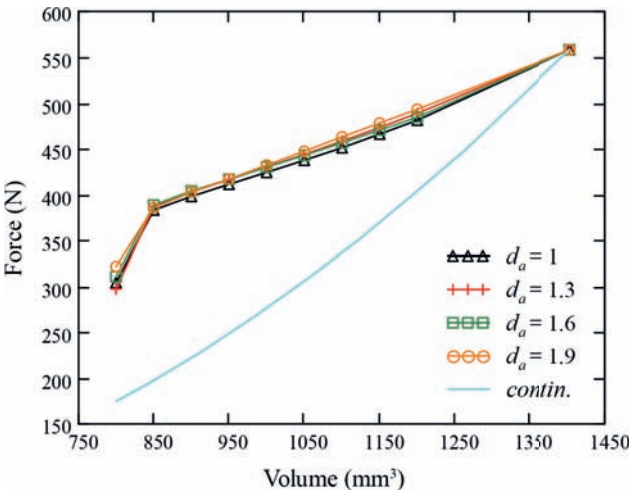


*Figure 12. Diagram of the solid body volume of composite and solid plates dependence of the load $F_y$ (at $\sigma_{max} = \sigma_{0.2}$) under three-point bending* (2)

## CONCLUSIONS

Based on the results of the numerical analysis, it has been shown that composite plates with tetrachiral honeycombs with a relative density of honeycomb cores from 20 to 70% have a significantly higher strength relative to solid plates with an equal volume of a solid body. At

bending with rigid fixation, the discretization of tetrachiral structures effects the strength of composite plates at relative density values from 20 to 35%. Honeycombs with large unit cell size are stronger relative to those with smaller unit cell size at the same relative density. The use of tetrachiral honeycomb cores in the design of composite plates is a promising approach for improving the mechanical properties of composite plates.

## FUNDING

This research has been supported by the Project #3.1.1.2 within the 2021 Plan of Fundamental Research of the Russian Academy of Architecture and Civil Engineering and Ministry of Civil Engineering and Public Utilities of the Russian Federation. The studies have been carried out using the facilities of the Collective Research Center named after Professor Yu. M. Borisov, Voronezh State Technical University, which is partly supported by the Ministry of Science and Education of the Russian Federation, Contract No 075- 15-2021-662.

## REFERENCES

1. **Saxena K.K., Das R., Calius E.P.** Three decades of auxetics research – materials with negative Poisson's ratio: a review // Advanced Engineering Materials, 2016, Vol. 18, pp. 1847-1870. DOI:10.1002/adem.201600053
2. **Lakes R.S.** Negative-Poisson's-ratio materials: auxetic solids // Annual review of materials research, 2017, Vol. 47, pp. 63-81. DOI:10.1146/annurev-matsci-070616-124118
3. **Wang Z., Luan C., Liao G., Liu J., Yao X., Fu J.** Progress in auxetic mechanical metamaterials: structures, characteristics, manufacturing methods, and applications // Advanced Engineering Materials, 2020, Vol. 22, Article ID 2000312. DOI:10.1002/adem.202000312
4. **Love A.E.H.** A treatise on the mathematical theory of elasticity // Cambridge University Press, Cambridge, 1892. https://hal.archives-ouvertes.fr/hal-01307751
5. **Landau L.D., Lifshitz E.M.** Course of Theoretical Physics Vol 7: Theory and Elasticity // Pergamon Press, Oxford, 1959**.**
6. **Mazaev A.V., Ajeneza O., Shitikova M.V.** Auxetics materials: classification, mechanical properties and applications // IOP Conference Series: Materials Science and Engineering, 2020, Vol. 747, p. 012008. DOI:10.1088/1757-899X/747/1/012008
7. **Prall D., Lakes R.S.** Properties of a chiral honeycomb with a Poisson's ratio of -1 // International Journal of Mechanical Sciences, 1997, Vol. 39, pp. 305-314. DOI:10.1016/S0020-7403(96)00025-2
8. **Scarpa F.L., Tomlinson G.R.** Vibroacoustics and damping analysis of negative Poisson's ratio honeycombs // Proceedings of SPIE, Smart Structures and Materials: Passive Damping and Isolation, 1998, Vol. 3327, pp. 339-348. DOI:10.1117/12.310695
9. **Alderson A., Alderson K.L., Attard D., Evans K.E., Gatt R., Grima J.N., Miller W., Ravirala N., Smith C.W., Zied K.** Elastic constants of 3-, 4-and 6-connected chiral and anti-chiral honeycombs subject to uniaxial in-plane loading // Composites Science and Technology, 2010, Vol. 70, pp. 1042-1048. DOI:10.1016/j.compscitech.2009.07.009
10. **Lira C., Scarpa F., Rajasekaran R.** A gradient cellular core for aeroengine fan blades based on auxetic configurations // Journal of Intelligent Material Systems and Structures, 2011, Vol. 22, pp. 907-917. DOI:10.1177/1045389X11414226
11. **Li T., Wang L.** Bending behavior of sandwich composite structures with tunable 3D-printed core materials // Composite Structures, 2017, Vol. 175, pp. 46-57. DOI:10.1016/j.compstruct.2017.05.001
12. **Alomarah A., Masood S.H., Sbarski I., Faisal B., Gao Z., Ruan D.** Compressive

properties of 3D printed auxetic structures: experimental and numerical studies // Virtual and Physical Prototyping, 2020, Vol. 15, pp. 1-21. DOI:10.1080/17452759.2019.1644184

13. **Xiao D., Chen X., Li Y., Wu W., Fang D.** The structure response of sandwich beams with metallic auxetic honeycomb cores under localized impulsive loading-experiments and finite element analysis // Materials & Design, 2019, Vol. 176, p. 107840. DOI:10.1016/j.matdes.2019.107840
14. **Essassi K., Rebiere J.L., El Mahi A., Ben Souf M.A., Bouguecha A., Haddar M.** Investigation of the static behavior and failure mechanisms of a 3D printed bio-based sandwich with auxetic core // International Journal of Applied Mechanics, 2020, Vol. 12, p. 2050051. DOI:10.1142/S1758825120500519
15. **Smardzewski J.** Experimental and numerical analysis of wooden sandwich panels with an auxetic core and oval cells // Materials & Design, 2019, Vol. 183, p. 108159. DOI:10.1016/j.matdes.2019.108159
16. **Peliński K., Smardzewski J.** Bending behavior of lightweight wood-based sandwich beams with auxetic cellular core // Polymers, 2020, Vol. 12, p. 1723. DOI:10.3390/polym12081723
17. COMSOL AB. Structural Mechanics Module User's Guide // COMSOL AB, Stockholm, 2020
18. **Shalin R.E.** Aviation materials: reference book. Aluminum and beryllium alloys. Deformable aluminum alloys and beryllium-based alloys (in Russian) // VIAM, Moscow, 1982.
19. **Obraztsov I.F., Savel'ev L.M., Khazanov K.S.** Finite element method in problems of structural mechanics of aircraft (in Russian) // Vysshaya Shkola, Moscow, 1985.
20. **Zienkiewicz O.C., Morice P.B.** The finite element method in engineering science // McGraw-Hill, London, 1971.
21. **Rabotnov Yu.N.** Resistance of materials (in Russian) // Fizmatgiz, Moscow, 1962.

## СПИСОК ЛИТЕРАТУРЫ

1. **Saxena K.K., Das R., Calius E.P.** Three decades of auxetics research – materials with negative Poisson's ratio: a review // Advanced Engineering Materials, 2016, Vol. 18, pp. 1847-1870. DOI:10.1002/adem.201600053
2. **Lakes R.S.** Negative-Poisson's-ratio materials: auxetic solids // Annual review of materials research, 2017, Vol. 47, pp. 63-81. DOI:10.1146/annurev-matsci-070616-124118
3. **Wang Z., Luan C., Liao G., Liu J., Yao X., Fu J.** Progress in auxetic mechanical metamaterials: structures, characteristics, manufacturing methods, and applications // Advanced Engineering Materials, 2020, Vol. 22, Article ID. 2000312. DOI:10.1002/adem.202000312
4. **Ляв А.** Математическая теория упругости // М.-Л.: ОНТИ, 1935.
5. **Ландау Л.Д., Лифшиц Е.М.** Механика сплошных сред. Гидродинамика и теория упругости // М.-Л.: Гостехиздат, 1944.
6. **Mazaev A.V., Ajeneza O., Shitikova M.V.** Auxetics materials: classification, mechanical properties and applications // IOP Conference Series: Materials Science and Engineering, 2020, Vol. 747, p. 012008. DOI:10.1088/1757-899X/747/1/012008
7. **Prall D., Lakes R.S.** Properties of a chiral honeycomb with a Poisson's ratio of -1 // International Journal of Mechanical Sciences, 1997, Vol. 39, pp. 305-314. DOI:10.1016/S0020-7403(96)00025-2
8. **Scarpa F.L., Tomlinson G.R.** Vibroacoustics and damping analysis of negative Poisson's ratio honeycombs // Proceedings of SPIE, Smart Structures and Materials: Passive Damping and Isolation, 1998, Vol. 3327, pp. 339-348. DOI:10.1117/12.310695
9. **Alderson A., Alderson K.L., Attard D., Evans K.E., Gatt R., Grima J.N., Miller W., Ravirala N., Smith C.W., Zied K.** Elastic constants of 3-, 4-and 6-connected chiral and

anti-chiral honeycombs subject to uniaxial in-plane loading // Composites Science and Technology, 2010, Vol. 70, pp. 1042-1048. DOI:10.1016/j.compscitech.2009.07.009
10. **Lira C., Scarpa F., Rajasekaran R.** A gradient cellular core for aeroengine fan blades based on auxetic configurations // Journal of Intelligent Material Systems and Structures, 2011, Vol. 22, pp. 907-917. DOI:10.1177/1045389X11414226
11. **Li T., Wang L.** Bending behavior of sandwich composite structures with tunable 3D-printed core materials // Composite Structures, 2017, Vol. 175, pp. 46-57. DOI:10.1016/j.compstruct.2017.05.001
12. **Alomarah A., Masood S.H., Sbarski I., Faisal B., Gao Z., Ruan D.** Compressive properties of 3D printed auxetic structures: experimental and numerical studies // Virtual and Physical Prototyping, 2020, Vol. 15, pp. 1–21. DOI:10.1080/17452759.2019.1644184
13. **Xiao D., Chen X., Li Y., Wu W., Fang D.** The structure response of sandwich beams with metallic auxetic honeycomb cores under localized impulsive loading-experiments and finite element analysis // Materials & Design, 2019, Vol. 176, p. 107840. DOI:10.1016/j.matdes.2019.107840
14. **Essassi K., Rebiere J.L., El Mahi A., Ben Souf M.A., Bouguecha A., Haddar M.** Investigation of the static behavior and failure mechanisms of a 3D printed bio-based sandwich with auxetic core // International Journal of Applied Mechanics, 2020, Vol. 12, p. 2050051. DOI:10.1142/S1758825120500519
15. Smardzewski J. Experimental and numerical analysis of wooden sandwich panels with an auxetic core and oval cells // Materials & Design, 2019, Vol. 183, Article ID 108159. DOI:10.1016/j.matdes.2019.108159
16. **Peliński K., Smardzewski J.** Bending behavior of lightweight wood-based sandwich beams with auxetic cellular core // Polymers, 2020, Vol. 12, p. 1723. DOI:10.3390/polym12081723
17. COMSOL AB. Structural Mechanics Module User's Guide // COMSOL AB, Stockholm, 2020
18. **Шалин Р.Е.** Авиационные материалы. Алюминиевые и бериллиевые сплавы. Деформируемые алюминиевые сплавы и сплавы на основе бериллия // М.: ОНТИ, 1982.
19. **Образцов И.Ф., Савельев Л.М., Хазанов Х.С.** Метод конечных элементов в задачах строительной механики летательных аппаратов // М.: Высшая школа, 1985.
20. **Зенкевич О.** Метод конечных элементов в технике. М.: Мир, 1975.
21. **Работнов Ю.Н.** Сопротивление материалов // М.: Физматгиз, 1962.

*Alexey V. Mazaev*, PhD Student, Junior Researcher, Research Center on Dynamics of Solids and Structures; Voronezh State Technical University; 84, 20-letija Oktyabrya, Voronezh, 394006, Russia; Reserach Engineer, RAASN Research Institute of Structural Physics, Moscow, Russia. E-mail: mazaevonline@gmail.com.

*Marina V. Shitikova*, Advisor of the Russian Academy of Architecture and Construction Sciences, Prof., Dr. Sc., Research Center on Dynamics of Solids and Structures; Voronezh State Technical University; 84, 20-letija Oktyabrya, Voronezh, 394006, Russia; phone +7 (473) 271-52-68; fax +7 (473) 271-52-68; Senior Researcher, RAASN Research Institute of Structural Physics, Moscow, Russia. E-mail: mvs@vgasu.vrn.ru.

*Мазаев Алексей Вячеславович*, аспирант; младший научный сотрудник научного Центра по фундаментальным исследованиям в области естественных и строительных наук; Воронежский государственный технический университет; 394006, Россия, г. Воронеж, ул. 20 лет Октября, д. 84; инженер-исследователь, Научно-исследовательский институт строительной физики РААСН, Москва, Россия. E-mail: mazaevonline@gmail.com.

*Шитикова Марина Вячеславовна*, советник РААСН, профессор, доктор физико-математических наук; руководитель международного научного Центра по фундаментальным исследованиям в области естественных и строительных наук; Воронежский государственный технический университет; 394006, Россия, г. Воронеж, ул. 20 лет Октября, д. 84, тел. +7 (473) 271-52-68; факс +7 (473) 271-52-68; Главный научный сотрудник, Научно-исследовательский институт строительной физики РААСН, Москва, Россия. E-mail: mvs@vgasu.vrn.ru.